The Linkage Between the Ring Current and the Ionosphere System

P. C. Brandt, Y. Zheng, and T. S. Sotirelis

The Johns Hopkins University Applied Physics Laboratory, Laurel, Maryland, USA

K. Oksavik

The University Center in Svalbard, Longyearbyen, Norway

F. J. Rich

Air Force Research Laboratory, Acton, Massachusetts, USA

The coupling between the ring current and the ionosphere is briefly reviewed and discussed. Given global energetic neutral atom (ENA) observations of the ring current, the three-dimensional current system driven by ring current plasma pressure (the region 2 system) is derived to illustrate where the ring current connects to the ionosphere. Special attention is given to how the ring current and ionospheric conductance set up the sub-auroral polarization streams (SAPS) through the closure of the region 2 current through the ionospheric trough region. Simultaneous ENA observations of the ring current and radar observations of the SAPS flow show that the onset of SAPS flow and equatorward motion is coincident with the injection and buildup of plasma pressure in the inner magnetosphere. The comprehensive ring current model is used to demonstrate how the SAPS can be generated by computing ring current pressure and allowing its pressure-driven currents to close through a model of ionospheric conductance including the trough region. The paper ends by discussing open questions and what is missing in our understanding of the generation of the large-scale electric fields of the inner magnetosphere and sub-auroral ionosphere.

1. INTRODUCTION

Phenomena in near-Earth space stem from an intrinsically coupled system of plasmas and fields. To understand phenomena in the magnetosphere, ionosphere, and even the thermosphere, we must understand how these systems work together to produce the phenomena we observe. The plasma pressure of the ring current is by far the largest source of inner magnetospheric currents (region 2 current system) that couple through the ionosphere and is therefore critical to the magnetosphere–ionosphere coupling process. The closure of the magnetospheric currents through the ionospheric conductance pattern give rise to the large-scale electric field of the magnetosphere as well as the ionosphere and can therefore be viewed as an important input to thermospheric phenomena. The picture is further complicated by the fact that the thermosphere modifies ionospheric conductance.

The purpose of this paper is to give a brief review of our knowledge on how the ring current couples to the ionosphere

Midlatitude Ionospheric Dynamics and Disturbances
Geophysical Monograph Series 181

10.1029/181GM13

and the effects that arise. We begin by giving a brief background to storm-time ring current dynamics in section 2. In section 3, we discuss the global picture of the ring current–ionosphere coupling, and continue presenting observations on the effects of this coupling, as exemplified by the subauroral polarization stream (SAPS).

2. RING CURRENT DYNAMICS

Historically, the ring current has been thought of as a ring of electrical current encircling the Earth. However, recent global energetic neutral atom (ENA) observations of the ring current by the IMAGE mission [*Burch*, 2000] have noted that the storm-time ring current is highly asymmetric with its center on the night side [*Brandt et al*., 2002]. Observations by IMAGE have enabled investigations of the global dynamics of not only the ring current through ENA imaging but also of the plasmasphere [*Goldstein et al.*, 2005], which can be used as a tracer of the electric field of the inner magnetosphere.

Plate 1 demonstrates how dynamic the ring current really is. The ENA image sequence was obtained via the high energy neutral atom (HENA) imager [*Mitchell et al.*, 2000] on 24 November 2001 during a transition from a geomagnetic storm main phase to a recovery phase. The hydrogen ENA images are integrated for 20 min and are obtained in the 60- to 119-keV range, which represents the bulk of the plasma pressure in the ring current.

The peak of the storm was reached at about 1444 UTC and the southward interplanetary magnetic field (IMF) turned northward at Earth at about 1500 UTC. Within minutes, the ring current began to respond by becoming more symmetric. This is due to the different drift patterns in the magnetosphere during northward IMF, during which the dominating drift is curvature and gradient drift. Drift trajectories then circle the Earth and energy dispersion, and charge exchange decay helps in azimuthally smoothing out spatial gradients in the ring current plasma pressure.

At 1618 UTC the ring current had already become significantly symmetric, and at 1752 UTC it was almost entirely symmetric. Note that the *SYM-H* index is very negative large throughout this transition, which justifies strong caution that *SYM-H* does not always represent the state of the ring current accurately. The clear conclusion of these observations is that the ring current is *not* a ring during the driving phase of the storm [*Brandt et al.*, 2002; *Ebihara and Ejiri*, 2000; *Ebihara et al.*, 2002].

3. COUPLING AND ITS EFFECTS

The key quantity of the ring current is the plasma pressure carried mostly by protons and O^+ as shown by *Krimigis et al.* [1985]. The plasma pressure gradients are responsible for most of the electric current in the ring current. Contrary to some literature, the *equatorial* magnetospheric ring current is *not* dominated by the ions curvature and gradient drifting westward and the electrons eastward. Although this does give rise to a net westward current, it is a negligible effect on the currents perpendicular to the magnetic field for an isotropic plasma pressure distribution. Under such condition, the perpendicular current is dominated by the gradients of the perpendicular component of the pressure (the so-called diamagnetic current). See, for example, *Parker* [1957] for a complete derivation from single particle motion to electrical currents. One can show that the basic force balance equation for the ring current is

$$\mathbf{J} \times \mathbf{B} = \nabla \cdot \mathbf{P}. \tag{1}$$

Note that this equation only gives us information about the currents perpendicular to the magnetic field. To visualize the electrical current flow lines of the inner magnetosphere, one can assume current continuity $\nabla \cdot \mathbf{J} = 0$. Combining this with the force balance equation (1), one may derive the three-dimensional system of currents connecting to the ionosphere. For a more detailed treatment, see *Roelof* [1987].

The result of this exercise is displayed in Plate 2. The storm-time ring current plasma pressure is displayed in the magnetic equator and is distributed around the midnight sector. The pressure is retrieved from HENA images by using a constrained linear inversion algorithm [*DeMajistre et al.*, 2004]. The electric current flow lines have been plotted for one iso-pressure surface and are shown as dashed lines. The complete ring current system is built up of an infinite number of such iso-pressure surfaces and is commonly known as the region 2 current system.

In the equator, the current flow lines close on themselves and there are no field-aligned currents (FAC) flowing. The magnetospheric equatorial current is large and westward on the outer edge of the ring current pressure peak, but is much smaller and eastward on the inside edge of the ring current pressure. At higher latitudes, the FAC component increase and the current flow lines start to connect to the ionosphere. Currents flow into the ionosphere on the dusk side and up through the dawn side sector.

Note that the solution does permit a constant interhemispheric FAC that we have set to zero for simplicity. Independent in situ measurements confirm that the FAC density is indeed small near the equatorial plane and that there may be an interhemispheric current present [*Vallat et al.*, 2005].

In the dusk and dawn side ionosphere, the Pedersen conductance dominates so that the region 2 FAC currents close poleward (equatorward) at dusk (dawn) through the region

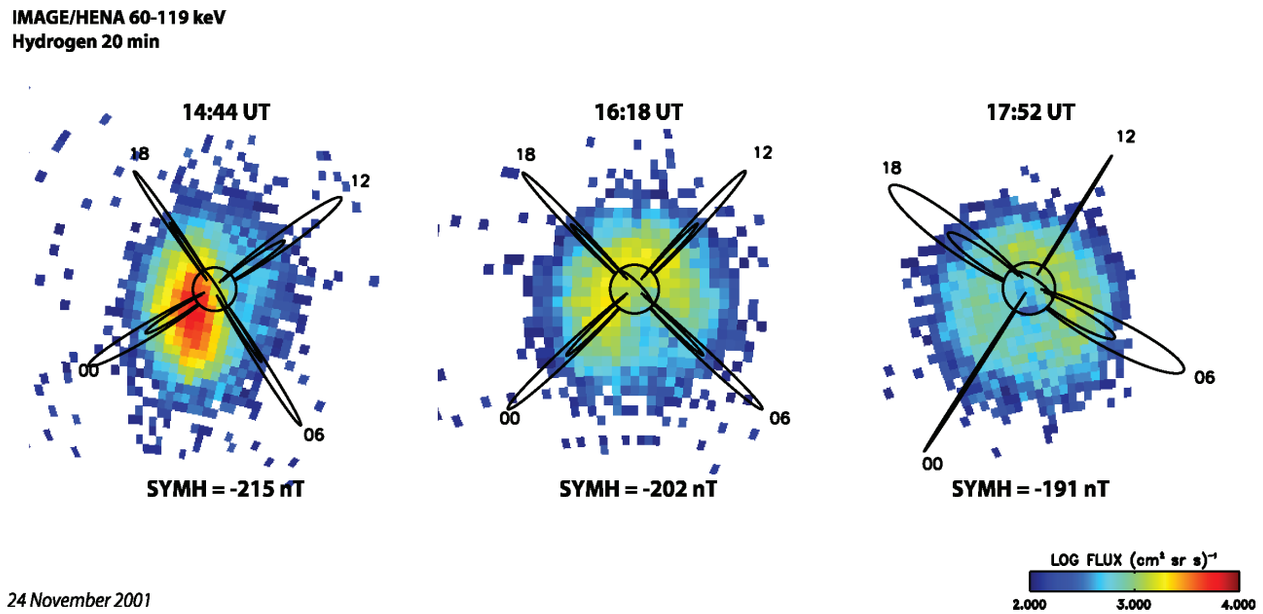

Plate 1. The ENA image sequence obtained by the high energy neutral atom (HENA) imager on board the IMAGE spacecraft. The sequence was obtained during a transition from the storm main phase to the storm recovery phase. The interplanetary magnetic field turned from southward to northward at about 1500 UTC and within minutes the ring current responded by becoming more symmetric.

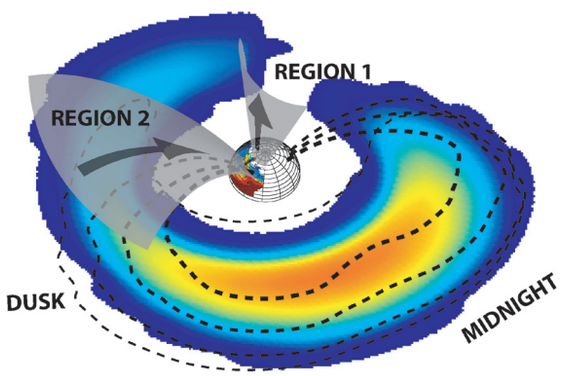

Plate 2. The ring current plasma pressure drives an electrical current system ("region 2") that closes through the dusk and dawn side ionosphere during storms. This global electrical circuit is a significant player in producing the sub-auroral polarization streams (SAPS) in the dusk side ionosphere, and is also responsible for modifying the electric field of the inner magnetosphere.

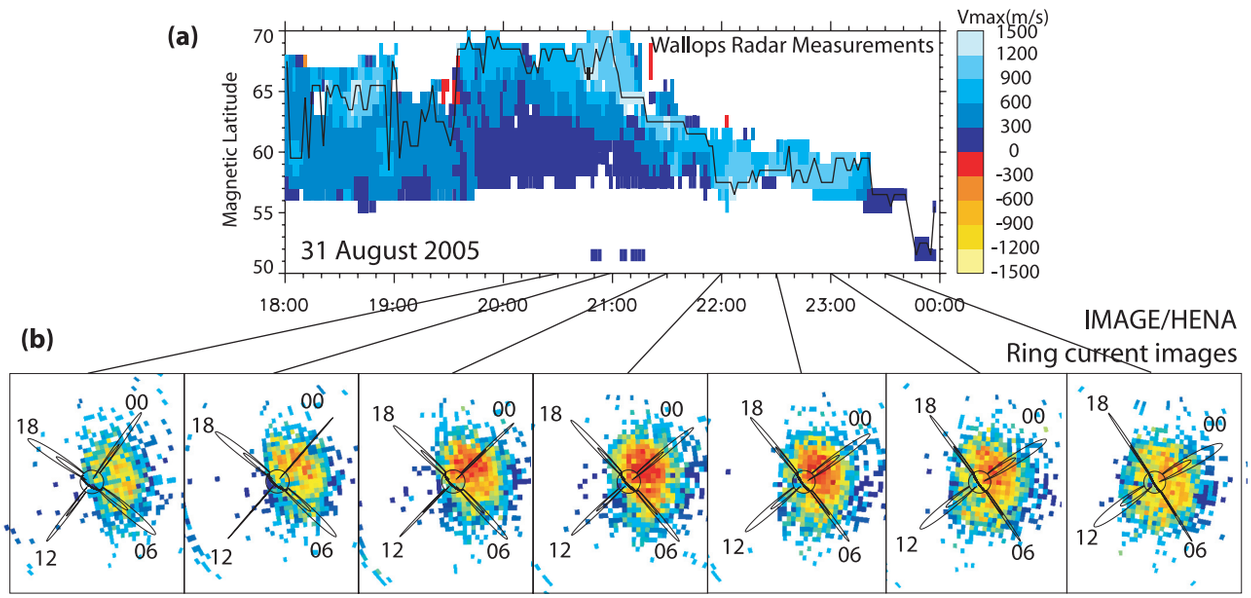

Plate 3. (a) The color coded line-of-sight (LOS) velocities as a function of magnetic latitude and UTC. The black line marks maximum LOS velocity. (b) The HENA image sequence in the 60- to 198-keV range.

1 current system. Let us here focus on what happens on the dusk side. Here, the ionospheric currents close through the low-conductance ionospheric trough region, which sets up a poleward electric field associated with enhanced ionospheric plasma flow velocities ($\mathbf{E} = -\mathbf{v} \times \mathbf{B}$) commonly referred to as SAPS [*Foster and Burke*, 2002].

The trough is present at quiet times and is formed through the stagnation of plasma in the region where the two-cell convection speed meets the corotating ionospheric plasma [*Spiro et al.*, 1978]. The result is an increased recombination rate and extremely low conductances (tenths of a mho). As convection increases due to a southward IMF, the two-cell convection pattern expands to lower latitudes and pushes the trough region with it.

There are numerous observations of the enhanced flow velocities associated with the SAPS phenomena made from both in situ spacecraft and remote radar observations [*Foster and Burke*, 2002; *Anderson et al.*, 2001]. Now with the addition of global ENA data and modeling efforts, a more complete picture of the SAPS mechanism is beginning to emerge. The ring current closure through the trough region plays a central role in producing the high-speed flows. On one hand, for a given trough conductance and location, the ring current strength determines the speed of the SAPS flow. On the other hand, *Anderson* [2004] demonstrated that the relative location of the trough and the aurora plays a significant role, which can be intuitively explained since their relative locations determine the distance the ionospheric current has to flow, which directly relates to the total resistance. Also, *Brandt et al.* [2005] demonstrated that the relative location may be the controlling effect of the SAPS velocity more than the FAC current density.

Plate 3 shows remote radar measurements of the flow velocities with simultaneous global ring current observations, suggesting that the ring current plays an active role in the formation and evolution of the SAPS. Plate 3a shows the line-of-sight (LOS) velocities of the SAPS flow during an event on 31 August 2005 (black line). The measurements were obtained by the SuperDARN radar facility on Wallops Island, VA [*Oksavik et al.*, 2006]. Plate 3a shows color-coded LOS velocities versus magnetic latitude and UTC. Plate 3b shows the corresponding HENA images for this period. All HENA images were integrated for 20 min. It is also possible to derive the actual three-dimensional current system for this period [*Roelof et al.*, 2004], but that is beyond the scope of this paper.

The ring current shows a sharp increase just before the enhancement of the SAPS flow velocities at about 2040 UTC. The SAPS velocity is maintained at a high level and the magnetic latitude of the SAPS channel decreases as ring current intensity continues to increase. *Foster and Burke* [2002] found that the magnetic latitude of the SAPS flow velocity decreases with increasing magnetic local time. We cannot rule out that the observed decrease in latitude is a spatial effect. There are other temporal effects that may cause the same phenomena. First of all, the auroral oval moves to lower latitudes during storms. Second, the ring current moves closer to Earth during storms, which would cause the region 2 FAC system to move to lower latitudes. At this point, we cannot separate these effects in the observations.

At about 2200 UTC the ring current intensity decreases, which is immediately reflected in the magnetic latitude of the SAPS, but not as much in the SAPS velocity. We cannot rule out that the decrease in magnetic latitude of the peak of SAPS flow velocity is a spatial effect as found by *Foster and Burke* [2002]. Keep in mind here that the plotted velocities are not the absolute SAPS velocity, but rather the LOS velocities derived from the radar measurements.

4. MODELING

Attempts to model the SAPS formation are not new. The Rice Convection Model (RCM) [*Wolf*, 1970; *Southwood and Wolf*, 1978] was among the first to illustrate the importance of ionospheric conductivity on magnetospheric and ionospheric flows. Other attempts include those reported by *Pintér et al.* [2006], *Lyatsky et al.* [2006], *Garner et al.* [2004], and *Harel et al.* [1981].

Today, most ring current models self-consistently compute the electric field in the ionosphere and magnetosphere by solving Poisson's equation for the pressure-driven currents closing through the ionosphere [*Fok et al.*, 2001; *Liemohn et al.*, 2006]. The equation provides the electric potential distribution in the ionosphere, which is assumed to be the same in the magnetosphere. The ionospheric and magnetospheric flow velocities are then simply computed as the $E \times B$ velocity. There are also recent important efforts to develop ring current models with a self-consistent magnetic field by computing the magnetic field deformation due to the pressure-driven currents [*Zaharia et al.*, 2006].

The comprehensive ring current model (CRCM) was developed by *Fok et al.* [2001] and is a further development of the RCM in that it computes the pitch-angle distributions by using the bounce averaged Boltzmann equation. The ionospheric conductance usually consists of three parts: (1) dayside conductance due to solar illumination, (2) nightside background conductance, and (3) auroral conductance. These conductances have usually been determined through statistical models such as the auroral conductance model by *Hardy et al.* [1985]. Figure 1a illustrates the magnetospheric electric fields resulting from a simple super position of the dawn to dusk electric field and the corotational electric field,

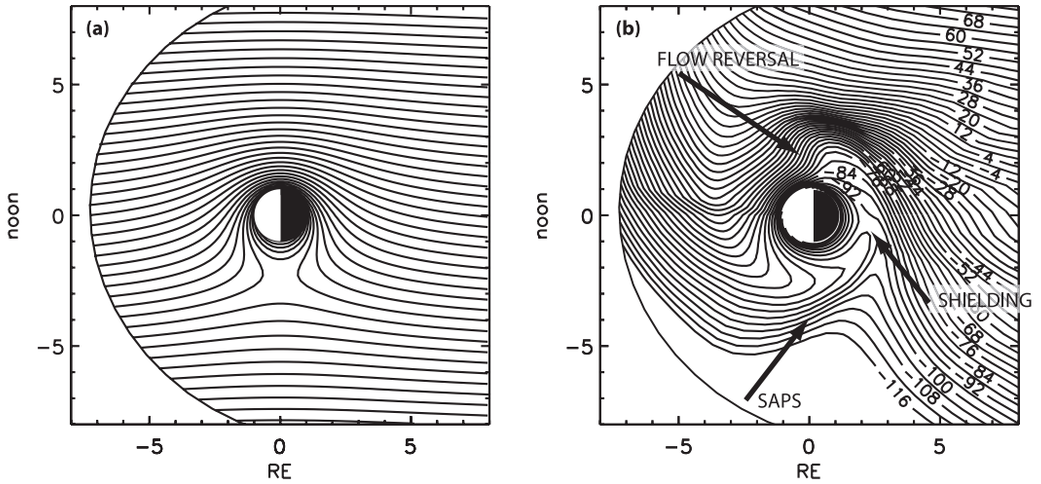

Figure 1. Closure of the pressure-driven current system through the ionosphere makes a dramatic difference on the magnetospheric and ionospheric electric field. (a) Electric potential pattern at the magnetic equator without current closure through the ionosphere. (b) Potential pattern from a typical comprehensive ring current model (CRCM) run (12 August 2000) allowing for current closure through the ionosphere.

representing the knowledge of the global distribution of storm-time electric fields of the inner magnetosphere before 1970. Figure 1b illustrates a typical storm-time CRCM run and demonstrates how a dramatically different electric field pattern arises when the model computes the electric field self-consistently. Even if the common statistical conductance models are heavily averaged and do not resolve the ionospheric trough region, the presence of an auroral oval on top of a lower background conductance reproduces a slightly enhanced SAPS flow velocity (200 m/s) at the equatorward edge of the auroral oval. Strong ionospheric and magnetospheric flows and electric fields are also known to exist on the dawn side [*Ebihara et al.*, 2005].

Zheng et al. [2008] implemented a *Kp*-driven empirical model of the ionospheric trough conductance [*Spiro et al.*, 1978] in the CRCM to determine the importance of the trough to SAPS formation for a storm period on 12 June 2005. In the present paper we have set the absolute conductance of the trough minimum to estimations from actual measurements by the Millstone Hill Incoherent Scatter Radar (P. Erickson and J. Foster, personal communication). Plate 4 summarizes the CRCM results and compares them to DMSP observations. Note that the CRCM model runs used a *Tsyganenko* [1995] model, which is strictly speaking a quiet-time magnetic field model. More accurate model runs will use a magnetic field model such as the *Tsyganenko and Sitnov* [2007] magnetic field model. We find that the following characteristics are important.

4.1. SAPS Velocity

With previous lack of realistic trough conductances, the CRCM reproduced much smaller SAPS flow velocities, and the region 2 FAC appeared slightly equatorward of the max SAPS flow. With the realistic trough conductances (dotted blue line in Plate 4), SAPS total flow velocities increase to about 2000 m/s (dotted red line), whereas the observed maximum cross-track velocity (solid red line) was 1400 m/s.

4.2. SAPS Location

The CRCM results clearly show that downward (positive) region 2 FAC (dotted black line), trough conductance (dotted blue line), and SAPS flow maximum (dotted red line) all coincide. The DSMP observations show a similar behavior where the region 2 FAC (gradient-filled boxed) coincides with the max of the SAPS flow maximum (solid red line). The background magnetic field has been subtracted to yield the plotted observed residual magnetic field (solid black line in the lower panel). We assume here that the FAC is sheet-like and extends in the east–west direction. The center of the current sheet will then be at the location where the residual magnetic field changes sign. No measured trough conductances were directly available for this date. However, from the total precipitating electron intensities (solid blue line in lower panel), we see that the observed SAPS flow maximum sits directly at the equatorward edge of the electron

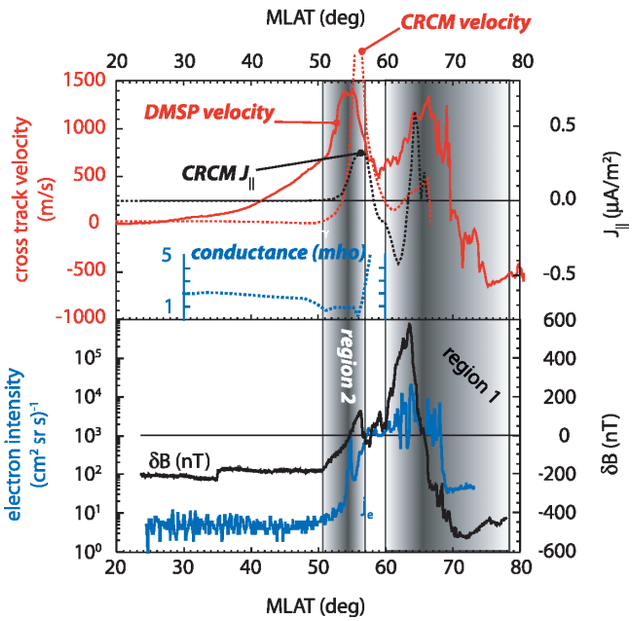

Plate 4. The location of the trough, the SAPS flow, and the region 2 field-aligned currents coincide. CRCM results are shown as dotted lines and DMSP measurements as solid lines.

precipitation, which is consistent with the location of the ionospheric trough.

5. DISCUSSION

Near-Earth space is an intrinsically coupled system of plasma and fields in the magnetosphere, ionosphere, and thermosphere. Although several sophisticated models can reproduce, at least qualitatively, phenomena such as the large-scale electric fields in the sub-auroral ionosphere and inner magnetosphere, it does not mean we understand how the different regions and regimes of space work together in reality to produce the observed phenomena. The SAPS phenomena is an excellent illustration: The modeled SAPS flow is reproduced by closing a current through an ionospheric conductance pattern with no feedback from the thermosphere. Yet, it is known that ionospheric conductance depends on the electric field [*Schunk and Walker*, 1973] through changes in thermospheric recombination rates. Therefore, the closure of the ring current across the ionospheric trough modifies the conductance, which in turn modifies the magnetospheric electric field. There are ongoing efforts to couple the inner magnetosphere, ionosphere, and thermosphere to understand this intrinsic coupling.

Furthermore, existing models of the SAPS flows are computed from the closure of currents through the ionosphere. However, we must not forget that the solar–wind magnetosphere interaction results in circulation of magnetized plasma in the magnetosphere, which imposes the two-cell convection pattern in the ionosphere. The ionospheric flow speeds depend on the ionospheric conductance. For a high ionospheric conductance, the convecting magnetic flux tubes will move slowly through the ionosphere (and speed up the plasma flow). At the lack of any significant conductance, flux tubes are free to move at high speeds (determined by the flow speeds in the magnetosphere). Therefore, the mere presence of an imposed flow and a low trough conductance will naturally result in a region with enhanced flows such as the SAPS flow. The SAPS electric field is then simply a consequence of the flow [*Vasyliūnas*, 2001], and the current system is set up to maintain the proper charge balance in accordance with the flow-induced electric field. This illustrates that the fundamental generation mechanism of the SAPS flow is a result of the complicated interaction between the magnetosphere and the ionosphere. Our interpretation, as manifested through the CRCM, represents a simplification of the entire system.

We have discussed ionospheric closure of the ring current as a way to explain the generation of SAPS flows. However, there are other important factors that impact the generation of the SAPS flow that we have not discussed in detail here. In summary, there are at least three factors that work together to create the large-scale electric field (or flow) of the inner magnetosphere/sub-auroral ionosphere:

1. *Flows*. The flows imposed on the ionosphere by magnetospheric convection depend on the ionospheric conductance. There are also thermospheric (neutral) wind-induced plasma flows that contribute to the ionospheric flows. It is still an open question how SAPS is affected by these flows.

2. *Currents*. The strength and morphology of the region 2 current system and where it closes through the ionosphere is critical in determining the ionospheric electric fields and flows. At present, this is the way most models compute the ionospheric electric fields due to ring current coupling. In a steady state, the currents, conductance, fields, and flows have to be consistent regardless of what drives what.

3. *Conductance*. It is clear that ionospheric conductance is of critical importance to the electric field, especially if it the conductance is low, as in the ionospheric trough region. In turn, changes in the thermosphere alter the ionospheric conductance in response to the flows and fields.

Acknowledgment. This work was supported by NASA grant NNX06AC29G.

REFERENCES

Anderson, P. C. (2004), Subauroral electric fields and magnetospheric convection during the April 2002 geomagnetic storms, *Geophys. Res. Lett.*, *31*, L11801, doi:10.1029/2004GL019588.

Anderson, P. C., D. L. Carpenter, K. Tsuruda, T. Mukai, and F. J. Rich (2001), Multisatellite observations of rapid subauroral ion drifts (SAID), *J. Geophys. Res.*, *106*(A12), 29,585–29,599.

Brandt, P. C., S. Ohtani, D. G. Mitchell, M.-C. Fok, E. C. Roelof, and R. DeMajistre (2002), Global ENA observations of the storm mainphase ring current: Implications for skewed electric fields in the inner magnetosphere, *Geophys. Res. Lett.*, *29*(20), 1954, doi:10.1029/2002GL015160.

Brandt, P. C., J. Goldstein, P. C. Anderson, B. J. Anderson, R. DeMajistre, E. C. Roelof, and D. G. Mitchell (2005), On the relation between sub-auroral electric fields, the ring current and the plasmasphere, *AGU Geophys. Monogr. Ser.*, *155*, 163–172.

Burch, J. L. (Ed.) (2000), *The IMAGE Mission*, Kluwer Academic, reprinted from *Space Sci. Rev.*, *91*(1–2).

DeMajistre, R., L. J. Paxton, D. Morrison, J.-H. Yee, L. P. Goncharenko, and A. B. Christensen (2004), Retrievals of nighttime electron density from thermosphere ionosphere mesosphere energetics and dynamics (timed) mission global ultraviolet imager (GUVI) measurements, *J. Geophys. Res.*, *109*, A05305, doi:10.1029/2003JA010296.

Ebihara, Y., and M. Ejiri (2000), Simulation study on the fundamental property of the storm-time ring current, *J. Geophys. Res.*, *105*, 15,843–15,859.

Ebihara, Y., M. Ejiri, H. Nilsson, I. Sandahl, A. Milillo, M. Grande, J. F. Fennell, and J. L. Roeder (2002), Statistical distribution of the storm-time proton ring current: POLAR measurements, *Geophys. Res. Lett.*, *29*(20), 1969, doi:10.1029/2002GL01540.

Ebihara, Y., M.-C. Fok, S. Sazykin, M. F. Thomsen, M. R. Hairston, D. S. Evans, F. J. Rich, and M. Ejiri (2005), Ring current and the magnetosphere–ionosphere coupling during the superstorm of 20 November 2003, *J. Geophys. Res.*, *110*, A09S22, doi:10.1029/2004JA010924.

Fok, M. C., R. A. Wolf, R. W. Spiro, and T. E. Moore (2001), Comprehensive computational model of Earth's ring current, *J. Geophys. Res.*, *106*(A5), 8417–8424.

Foster, J. C., and W. J. Burke (2002), SAPS: A new categorization for sub-auroral electric fields, *Eos Trans. AGU*, *83*(36), 393.

Garner, T. W., R. A. Wolf, R. W. Spiro, W. J. Burke, B. G. Fejer, S. Sazykin, J. L. Roeder, and M. R. Hairston (2004), Magnetospheric electric fields and plasma sheet injection to low L-shells during the 4–5 June 1991 magnetic storm: Comparison between the Rice Convection Model and observations, *J. Geophys. Res.*, *109*, A02214, doi:10.1029/2003JA010208.

Goldstein, J., J. L. Burch, B. R. Sandel, S. B. Mende, P. C. Brandt, and M. R. Hairston (2005), Coupled response of the inner magnetosphere and ionosphere on 17 April 2002, *J. Geophys. Res.*, *110,* A03205, doi:10.1029/2004JA010712.

Hardy, D. A., M. S. Gussenhoven, and E. Holeman (1985), A statistical model of auroral electron precipitation, *J. Geophys. Res.*, *90*(A5), 4229–4248.

Harel, M., R. A. Wolf, P. H. Reiff, R. W. Spiro, W. J. Burke, F. J. Rich, and M. Smiddy (1981), Quantitative simulation of a magnetospheric substorm: I. Model logic and overview, *J. Geophys. Res.*, *86*, 2217–2241.

Krimigis, S. M., G. Gloeckler, R. W. McEntire, T. A. Potemra, F. L. Scarf, and E. G. Shelley (1985), Magnetic storm of September 4, 1984: A synthesis of ring current spectra and energy densities measured with AMPTE/CCE, *Geophys. Res. Lett.*, *12*(5), 329–332.

Liemohn, M. W., A. J. Ridley, J. U. Kozyra, D. Gallagher, M. Thomsen, M. Henderson, M. Denton, P. C. Brandt, and J. Goldstein (2006), Analyzing electric field morphology through data-model comparisons of the geospace environment modeling inner magnetosphere/storm assessment challenge events, *J. Geophys. Res.*, *111*, A11S11, doi:10.1029/2006JA011700.

Lyatsky, W., A. Tan, and G. V. Khazanov (2006), A simple analytical model for subauroral polarization stream (SAPS), *Geophys. Res. Lett.*, *33*, L19101, doi:10.1029/2006GL025949.

Mitchell, D. G., et al. (2000), High energy neutral atom (HENA) imager for the IMAGE mission, *Space Sci. Rev.*, *91*, 67–112.

Oksavik, K., R. A. Greenwald, J. M. Ruohoniemi, M. R. Hairston, L. J. Paxton, J. B. H. Baker, J. W. Gjerloev, and R. J. Barnes (2006), First observations of the temporal/spatial variation of the sub-auroral polarization stream from the SuperDARN Wallops HF radar, *Geophys. Res. Lett.*, *33*, L12104, doi:10.1029/2006GL026256.

Parker, E. N. (1957), Newtonian development of the dynamical properties of ionized gases of low density, *Phys. Rev.*, *107*(4), 924–933.

Pintér, B., S. D. Thom, R. Balthazor, H. Vo, and G. J. Bailey (2006), Modeling subauroral polarization streams equatorward of the plasmapause footprints, *J. Geophys. Res.*, *111*, A10303, doi:10.1029/2005JA011457.

Roelof, E. C. (1987), Energetic neutral atom image of a storm-time ring current, *Geophys. Res. Lett.*, *14*, 652–655.

Roelof, E. C., P. C. Brandt, and D. G. Mitchell (2004), Derivation of currents and diamagnetic effects from global pressure distributions obtained by IMAGE/HENA, *Adv. Space Res.*, *33*(5), 747–751, doi:10.1016/S0273-1177(03)00633-1.

Schunk, R. W., and J. C. G. Walker (1973), Theoretical ion densities in the lower ionosphere, *Planet. Space Sci.*, *21*, 1875–1896, doi:10.1016/0032-0633(73)90118-9.

Southwood, D. J., and R. A. Wolf (1978), An assessment of the role of precipitation in magnetospheric convection, *J. Geophys. Res.*, *83*, 5227–5232.

Spiro, R. W., R. A. Heelis, and W. B. Hanson (1978), Ion convection and the formation of the mid-latitude *F* region ionization trough, *J. Geophys. Res.*, *83*, 4255–4264.

Tsyganenko, N. A. (1995), Modeling the Earth's magnetospheric magnetic field confined within a realistic magnetopause, *J. Geophys. Res.*, *100*, 5599–5612.

Tsyganenko, N. A., and M. I. Sitnov (2007), Magnetospheric configurations from a high-resolution data-based magnetic field model, *J. Geophys. Res.*, *112*, A06225, doi:10.1029/2007JA012260.

Vallat, C., et al. (2005), First current density measurements in the ring current region using simultaneous multi-spacecraft CLUSTER-FGM data, *Ann. Geophys.*, *23*, 1849–1865.

Vasyliūnas, V. M. (2001), Electric field and plasma flow: What drives what?, *Geophys. Res. Lett.*, *28*, 2177–2180, doi:10.1029/2001GL013014.

Wolf, R. A. (1970), Effects of ionospheric conductivity on convective flow of plasma in the magnetosphere, *J. Geophys. Res.*, *75*(25), 4677–4698.

Zaharia, S., V. K. Jordanova, M. F. Thomsen, and G. D. Reeves (2006), Self-consistent modeling of magnetic fields and plasmas in the inner magnetosphere: Application to a geomagnetic storm, *J. Geophys. Res.*, *111*, A11S14, doi:10.1029/2006JA011619.

Zheng, Y., P. Brandt, A. Lui, and M.-C. Fok (2008), On ionospheric trough conductance and subauroral ion drift: Simulation results, *J. Geophys. Res.*, *113*, A04209, doi:10.1029/2007JA012532.

P. C. Brandt, T. S. Sotirelis, and Y. Zheng, The Johns Hopkins University Applied Physics Laboratory, 11100 Johns Hopkins Rd, Laurel, MD 20723, USA. (pontus.brandt@jhuapl.edu)

K. Oksavik, The University Centre in Svalbard, NO-9171 Longyearbyen, Norway.

F. J. Rich, Air Force Research Laboratory, 15 Juniper Ridge Road, Acton, MA 01720, USA.